Probing ultrafast proton induced dynamics in transparent dielectrics

Probing ultrafast proton induced dynamics in transparent dielectrics

OPEN ACCESS
IOP Publishing
Plasma Physics and Controlled Fusion
Plasma Phys. Control. Fusion **60** (2018) 054004 (7pp)
https://doi.org/10.1088/1361-6587/aab16c

Probing ultrafast proton induced dynamics in transparent dielectrics

M Taylor[1], M Coughlan[1], G Nersisyan[1], L Senje[2], D Jung[1], F Currell[1], D Riley[1], C L S Lewis[1], M Zepf[1,3] and B Dromey[1]

[1] Centre for Plasma Physics, Queen's University Belfast, Belfast, BT7 1NN, United Kingdom
[2] Lund University, Department of Physics, PO Box 118, SE-221 00 Lund, Sweden
[3] Friedrich-Schiller-Universitt Jena, Föstengraben 1, D-07740, Jena, Germany

E-mail: b.dromey@qub.ac.uk

Received 27 November 2017, revised 9 February 2018
Accepted for publication 22 February 2018
Published 16 March 2018

Abstract

A scheme has been developed permitting the spatial and temporal characterisation of ultrafast dynamics induced by laser driven proton bursts in transparent dielectrics. Advantage is taken of the high degree of synchronicity between the proton bursts generated during laser-foil target interactions and the probing laser to provide the basis for streaking of the dynamics. Relaxation times of electrons ($<10^{-12}$ s) are measured following swift excitation across the optical band gap for various glass samples. A temporal resolution of <500 fs is achieved demonstrating that these ultrafast dynamics can be characterized on a single-shot basis.

Keywords: proton beams, ion acceleration, pump-probe, ultrafast dynamics

(Some figures may appear in colour only in the online journal)

Introduction

Experimental studies of ultrafast ($<10^{-12}$ s) atomic dynamics have become a reality [1] since the advent of high power, ultrashort laser systems [2, 3]. The ability to induce, tune and resolve dynamics on this time-scale has opened avenues of experimental research into regimes of nonlinear and relativistic optics [4–9]. To date, these have primarily focused on the use of ultrashort bursts of x-rays and electrons. However, following the demonstration of the generation of MeV proton beams via laser driven ion acceleration (LDIA) [10–17], recent work by Dromey *et al* [18] and Senje *et al* [19] has extended this to include the study of proton induced dynamics in matter. Beams of this type have unique and desirable qualities such as their high brightness [20] and ultra low longitudinal [21] and transverse [22] emittance. A range of applications have been proposed for these beams including hadron therapy [23] and fusion via proton-driven fast ignition [24].

Here we discuss a scheme, previously used to deduce the pulse duration of laser-driven proton bursts [18], which permits such characterisation by spatially and temporally overlapping proton bursts with a picosecond optical laser pulse and mapping the time dependent response of various samples to the irradiation. This work generalises the scheme outlined in [18] and details how this technique can be utilised in the study of ion interactions in any transparent dielectric for a wide range of material response times in either 2D or 1D. While such studies have been demonstrated for a wide range of radiation induced radiolysis processes [25–29], time-resolved studies employing proton pulses have not yet been carried out. Tracking the interaction of ultrafast ionisation sources in this manner requires high timing precision between the pump and the probe. Whilst attempts have been made to study the ultrafast responses via chemical scavenging techniques, the large concentrations of scavenger required to provoke such a fast response can result in high levels of uncertainty [30]. In the work described here, the versatility of the TARANIS [31] laser system was utilised to deliver synchronised high energy pump pulses for proton beam generation and lower energy pulses to probe the response of various glass samples. These

beams emanate from the same oscillator resulting in negligible timing jitter within the system.

Proton beam generation from laser interaction with matter relies on the formation of a hot electron cloud by an intense ($>10^{18}$ W cm^{-2}) laser incident on a solid target. These electrons are driven through the target via the ponderomotive force of the driving laser and set up a strong space charge field $\sim$TV m^{-1} on the rear side with the initially stationary ions. The resulting electrostatic trap then draws the relativistic electrons back in the direction of the target, permitting light ions to be preferentially accelerated into the vacuum. While other acceleration mechanisms have also been proposed as a source of LDIA [32, 33], this process, named target normal sheath acceleration (TNSA) [34], is the most commonly studied and implemented experimentally. TNSA beams are characterised by a Maxwellian-like spectrum with a sharp energy cutoff, depending on the laser intensity [34]. Stopping of proton beams produced by TNSA in bulk matter is the method used in this scheme to characterise the ultrafast sample response. Due to the broadband nature of the TNSA spectrum, an initially ultrashort proton pulse will be temporally stretched as it propagates in vacuum as a result of velocity dispersion. The intrinsic ultrashort pulse duration will, however, remain embedded in narrow energy slices of the spectrum and can be deduced from time of flight considerations of ions and the stopping power of the material under investigation [18].

The linear energy transfer (LET) of the protons as they propagate through the sample results in an energy spread proportional to depth along the propagation direction. The main distinction from the near homogeneous electron or photon irradiation is the production of nanometre (nm) wide ionisation tracks with steep energy density gradients as the protons lose their energy to valence band electrons [35, 36]. Track formation and excitation of valence band electrons to the conduction band occurs on timescales of attoseconds 10^{-18} s. Subsequent diffusion of the electrons homogenises the energy distribution over micrometre scale distances, leading to the existence of long lived ($>10^{-12}$ s) excited states. Probing the sample with 1 eV optical radiation during the interaction allows the electrons to take part in free–free absorption of the radiation [25] resulting in a reduced transmission of the probe. We define this mechanism as ion induced opacity. Relaxation to the valence band and the consequent end of the opacity is dependent on the crystalline structure and molecular composition of the samples. Synchronising the proton and probe pulses allowed for measurements of this relaxation time, t_r. Ionisation dynamics of different glass compounds were investigated by observation of the ion induced opacity. Tracking the response of matter to proton radiolysis generated by LDIA is crucial for potential applications to understand the dynamics on ultrafast timescales.

It is this mechanism which we employ to produce a generalised scheme which permits time resolved dynamics of the interaction. An outline of this is presented in figure 1. The TARANIS laser [31] (see Methods) was used to deliver high energy pulses to a flat foil target with a thickness of 12 μm for ion acceleration, whilst a lower energy probe was passed through various glass samples placed 5 mm from the Al target. Typical proton energies were first measured using radiochromic film (RCF) stacks and yielded a maximum energy of 10 $\pm$ 0.5 MeV. A 50 μm Al foil was placed on the front side of the sample to filter transmitted laser light and low energy electrons. Control of the relative delay between the pump and probe pulses was achieved by use of a delay line which had a range of $\pm$4 ns. After transmission through the sample, the probe beam could either be imaged straight onto a CCD or directed into a 1 m imaging spectrometer. Use of the former technique was applied only to transform limited (TL) probe pulses and is essentially a 2D snapshot of the interaction as in figure 2. While such a representation can be extremely useful to determine the proton diffusion at a specific instant, each of the samples exhibits a time-varying response dependent upon the crystalline structure which can exceed the length of the TL pulse. A full temporal depiction of the dynamics using this method could only be achieved by taking a series of 2D shots at incremental relative delays. While this is possible in principle, shot-to-shot variations in proton yield and energy restrict the accuracy of the results. This was addressed through the use of an optical streaking technique [37, 38], whereby adjusting the grating separation in the probe line compressor introduced a chirp, increasing the pulse duration. As the pulse is now stretched in time, each frequency will encounter a different level of opacity within the sample, thereby revealing the full temporal evolution of the material via frequency encoding of the opacity across the spectral range of the probe pulse. Adjusting the delay between the beams to compensate for this altering pulse length is necessary to ensure continued high degree of synchronisation between the pump and probe pulses.

Methods

TARANIS laser system

TARANIS is a hybrid Ti:Sapphire-Nd:glass laser system installed at Queen's University Belfast. The main beam has a FWHM pulse duration of 800 fs and delivers a maximum energy of 10 J onto a 12 μm thick Al target with a focal FWHM spot size of $\sim$5 μm correlating to intensities of 5×10^{18} W cm^{-2}. A lower energy probe pulse is picked off after the initial pre-amplification stage and compressed separately. The pulse duration can be controlled by changing the compressor grating separation, ΔL (see figure 1), allowing for flexibility with regards to the temporal window over which one can probe the dynamics. Proton beams are produced by the TNSA mechanism with maximum energy yields typically in the region of 10 $\pm$ 0.5 MeV. Energies were measured by stacks of RCF placed directly behind the Al target. To distinguish between protons and slower, co-propagating keV electrons, a 50 μm thick piece of aluminium

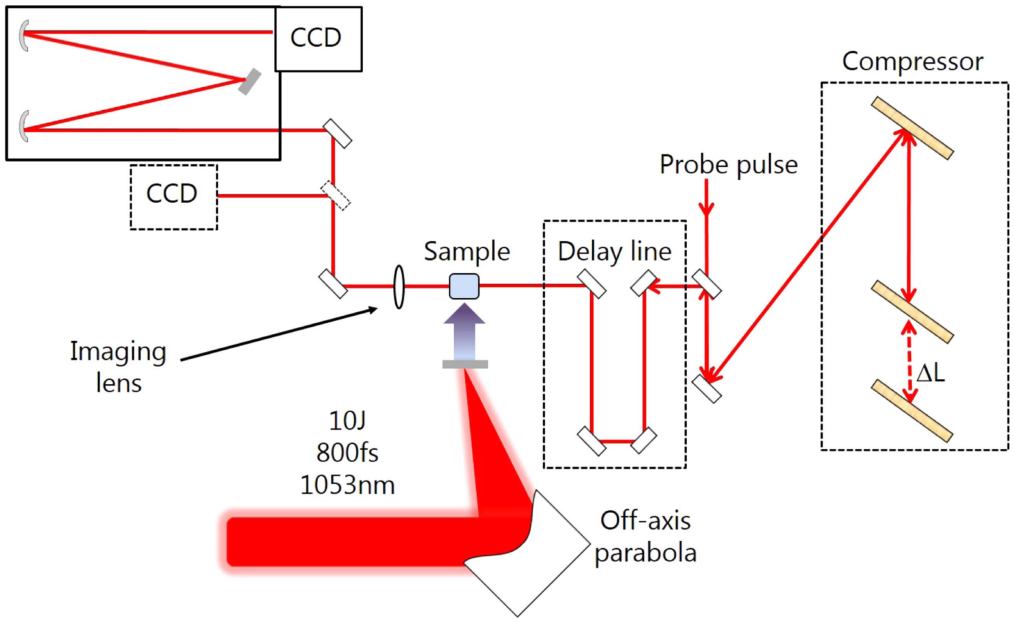

Figure 1. Schematic of the experiment. Experimental layout (not to scale). Both pump and probe pulses emanate from the same oscillator and are spatially and temporally synchronised in the interaction region. The lower energy probe beam is compressed separately whilst the pump undergoes further stages of amplification. The probe can be stretched by increasing the group delay dispersion of the pulse by changing the grating separation, ΔL. The lower limit pulse duration is the case when $\Delta L = 0$ corresponding to a transform limited duration of 470 fs with an upper limit of 1 ns obtained by bypassing the compressor. Although it is possible to utilise any pulse duration within this 1 ns range, for the results presented in this paper only durations of 470 fs, 50 ps, 200 ps and 1 ns are considered. A delay line is used to ensure the required delay between the beams. Ultrashort proton pulses are generated by the high energy laser pulse incident on a 10 μm Al foil placed 5 mm from the sample. A collimating slit and spectral filter are used to block keV electrons, x-rays and off-axis high energy protons (not pictured). After transmission through the sample, the probe beam can be imaged straight onto a CCD or using a grating spectrometer.

foil was placed directly in front of the sample to prevent the propagation of these electrons into the glass.

Wigner distributions (WDs)

The theoretical basis for the method of optical streaking can be understood by treating the electric field of the probe pulse in both the temporal and spectral domains simultaneously. WDs [39] are the simplest and most concise form of joint temporal and spectral representation, yielding information about the fractional field energy at any given time or for any given frequency component. For an electric field in the time domain $E(t)$, the WD is defined by

$$W(\omega, t) = \frac{1}{\pi}\int_{-\infty}^{\infty} E^*\left(t - \frac{\tau}{2}\right)E\left(t + \frac{\tau}{2}\right)e^{(i\omega\tau)}d\tau \qquad (1)$$

or spectrally as

$$W(\omega, t) = \frac{1}{\pi}\int_{-\infty}^{\infty} \tilde{E}^*\left(\omega - \frac{\Omega}{2}\right)\tilde{E}\left(\omega + \frac{\Omega}{2}\right)e^{(-i\Omega t)}d\Omega, \quad (2)$$

where $\tilde{E}(\omega)$ is the Fourier transform of $E(t)$. This expression allows for a mapping of the distribution of all frequency components as the pulse evolves over time. Such a representation is particularly important in the case of a chirped pulse where the group-delay dispersion (GDD) acts to aberrate the pulse from its TL duration, thereby staggering individual frequency components in time. For a chirped pulse initially of femtosecond duration with an electric field given by

$$\tilde{E}(\omega) = e^{-\left(\frac{T_{G0}}{2}\right)^2(\omega-\omega_0)^2}e^{i\frac{\beta}{2}(\omega-\omega_0)^2}, \qquad (3)$$

where $T_{G0} = T_P/\sqrt{2\ln 2}$, T_P is the FWHM of the TL pulse and β is the GDD term, an intensity normalised WD function was derived by Hong *et al* [40] and is given by

$$W(t, \omega) = \exp\left[-\frac{2}{T_{G0}^2}\left(t^2 - 2\beta\omega t + \frac{T_{G0}^4 + 4\beta^2}{4}\omega^2\right)\right]. \quad (4)$$

This expression was utilised to calculate the frequency distribution of a TL 470 fs pulse with a spectral bandwidth of 5.4 nm centred at 1053 nm, the results of which are presented in 3(a). No third order dispersion contributions are considered. When the grating separation in the compressor is increased by an amount ΔL, the GDD of the probe pulse increases yielding a longer pulse duration. The WD for a FWHM duration of 200 ps is presented in 3(b). As the frequency components of the pulse are spread over a greater temporal window the intensity distribution of the pulse narrows. Inducing such a chirp does not however sacrifice the temporal resolution of the TL pulse, as reported by Polli *et al* [38]. Therefore, for each of the pulse durations used in this scheme, the TL pulse duration of 470 fs is preserved for a given frequency. This is verified by figure 3(c). Taking a lineout across the central frequency (or indeed across any of the frequency components) reveals the embedded TL duration which is the limit of resolution for the scheme.

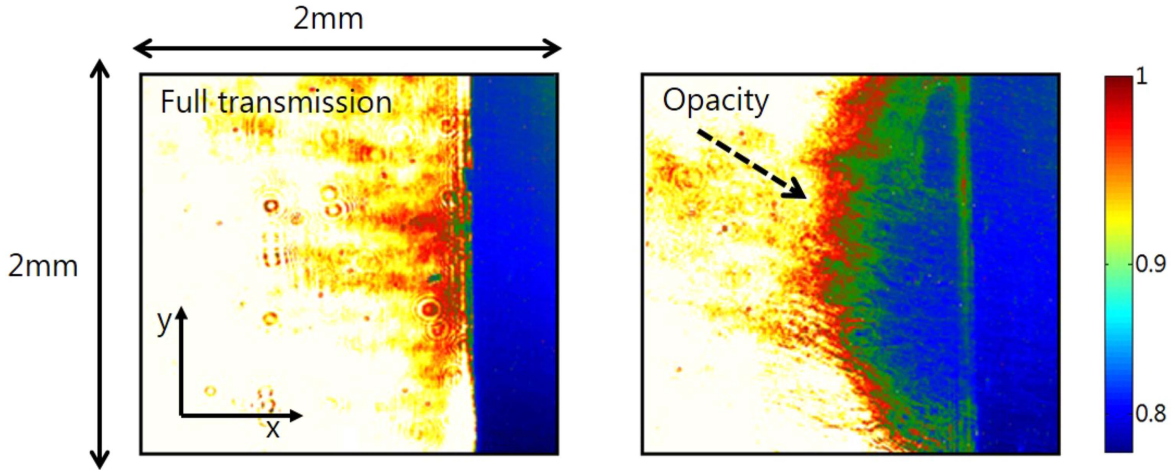

Figure 2. 2D snapshot with 470 fs integration time of ion induced opacity in BK7 glass. (a) is the case where no proton beam was incident on the sample and only the probe was passed through, corresponding to full transmission. The blue area on the right side of the image is the collimating slit placed before the sample. (b) is a snapshot of the damage induced by a proton beam at a time of 175 ps after the arrival of the main pulse at the surface of the Al target, T_0. The proton beam is incident from the right hand side.

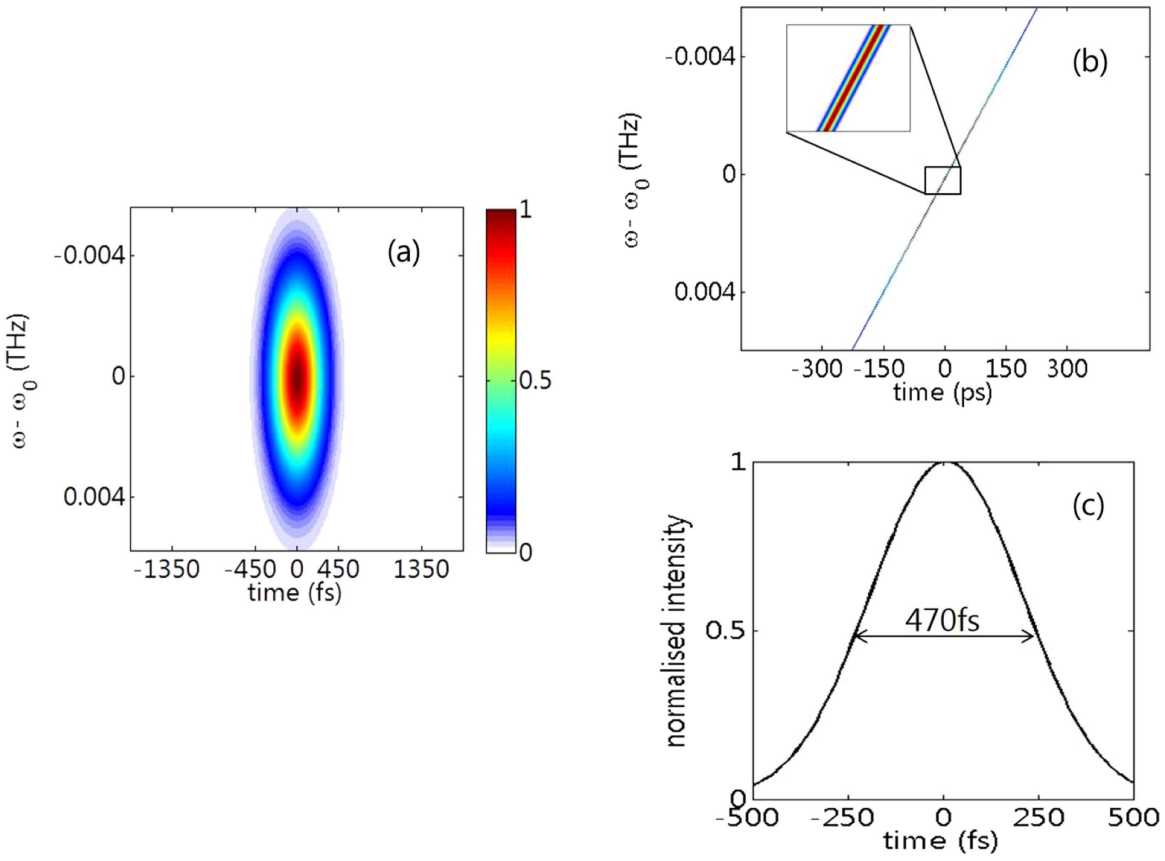

Figure 3. Normalised Wigner distributions. Transform limited probe pulse, (a), and for the case of a chirped pulse, (b), with FWHM pulse durations of 470 fs and 200 ps respectively. Inset of (b) is an enlarged image of the distribution around the central frequency (ω_0) detailing the intensity distribution. (c) is a spectral slice through (b) taken at ω_0 showing a FWHM pulse duration of 470 fs. This verifies that the ultimate temporal limit of resolution is the TL duration and that it is preserved for a chirped pulse at any given frequency component.

Results

Extending the temporal window

Initial probing of the samples using the fully compressed 470 fs probe provided a snapshot of the opacity within the sample as shown in figure 2 for borosilicate glass. Protons are incident upon the sample from the right side and are collimated to a width of 100 μm using an Al slit. Beyond this is the region of interest where the interaction between the ions and the sample takes place. With recombination times expected to be on the order of 100 s of ps [26], these

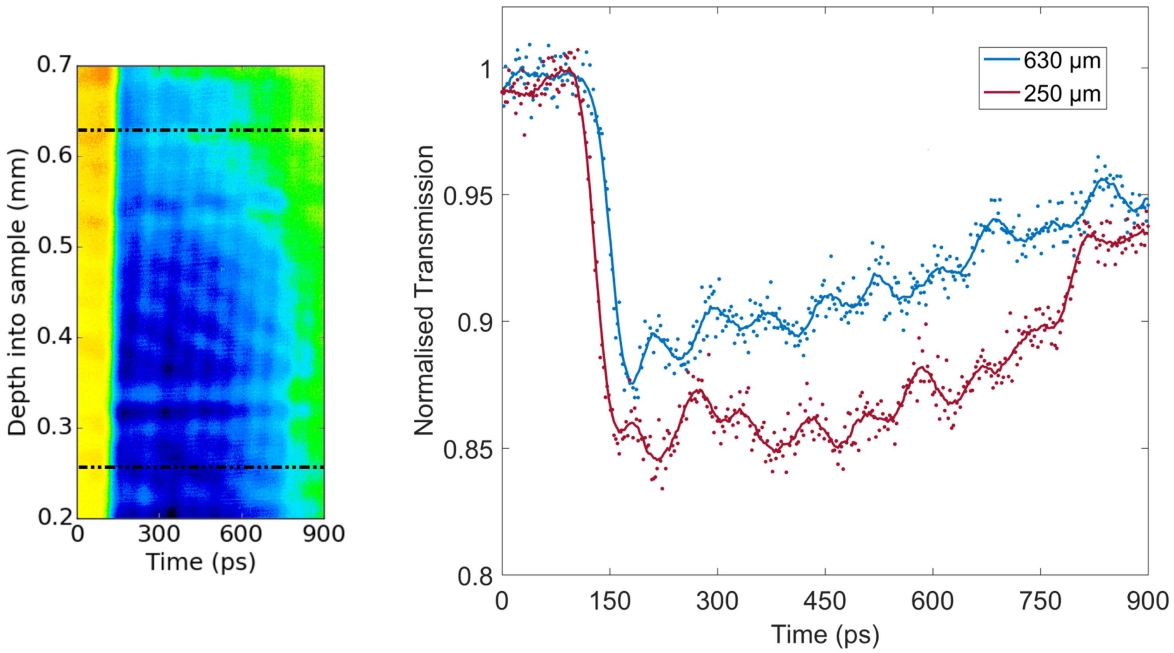

Figure 4. Optical streaking of ion induced opacity in Soda-lime glass. (a) Raw image of Soda-lime glass with a 1 ns probe beam. The arrival of the ion front occurs at a time of around 150 ps. Higher energy protons penetrate further into the sample as a result of lower LET and higher initial energy. The more abundant lower energy protons <5 MeV induce greater levels of opacity than that of the higher energy protons. The recovery to full transmission for the entire spectral range is also not evident before the end of the temporal window. By analysis of the depth of penetration and the temporal response, this method reveals the spatio-temporal information concurrently and details the entire interaction. (b) Lineouts taken for the entire temporal window corresponding to the stopping range for protons with initial energies of ∼5 and ∼10 MeV. Dots represent raw data points. Penetration depths for different proton energies estimated via SRIM calculations [42].

snapshots reveal the spatial diffusion of the ion beam at a specific instant and can capture the recovery with a number of subsequent shots at increasing delays. As mentioned previously, this technique is limited by shot-to-shot proton flux and energy fluctuations. By chirping the probe and using an imaging spectrometer, the complete temporal evolution of the sample dynamics can be resolved on a single shot basis, the added flexibility of this technique enables the observation of various material responses through the use of different probe pulse durations. Bypassing the probe compressor entirely permitted a 1 ns temporal window which enabled observation of long-lived responses, such as that of soda-lime glass shown in figure 4. Not shown is the contribution to the signal from protons with energies less than 5 MeV which have shorter penetration depths and the arrival of prompt relativistic x-ray/electron radiation, which is expected tens of picoseconds after the laser-target interaction. Therefore the delayed signal can only be due to energetic protons, as any lower energy electrons are removed by the aluminium foil. Arrival of the ion front and excitation of the electrons to the conduction band occurs rapidly, on the order of 10 ps. This feature is evident in figure 4(a) as the transmission sharply decreases to its minimum level. The transient opacity and consequent recovery of the sample to equilibrium is then recorded in this 1 ns window. Higher energy protons induce lower levels of opacity with a more rapid recovery to full transmission than signal due to lower energy contributions. This can be understood by considering the variation in the level of proton flux with energy. Due to the energy dependent stopping dynamics in the glass sample, it is possible to calculate the propagation depths for specific energy components and analyse the individual recombination times. In figure 4(b) the interaction at depths of 250 and 630 μm is presented. Opacity induced by protons of lower energy is maintained for longer due to a higher density of electrons occupying the conduction band, whilst a lower flux of protons at the highest energies means more rapid relaxation times.

Sample dependent response

By utilising samples of different crystalline structure and chemical composition, the differences in the lifetime of conduction band electrons could be established. Silicon dioxide (SiO_2) is another form of glass commonly used in laser line optic arrays with a higher damage threshold than that of soda-lime silica. Previous excitation studies on SiO_2 have observed a much more rapid response than that of the soda-lime glass. A mean free lifetime of the electrons on the order of 150 fs [25] has been previously proposed meaning much swifter recovery times.

Figure 5 shows the response of the sample over a 200 ps window at an energy of 8 MeV (see blue feature in insert). The onset of the opacity and recovery to full transmission lasts around 10 ps. This rapid response is two orders of magnitude quicker than the response observed in soda-lime glass. Once in the conduction band of SiO_2, the electrons quickly form self-trapped excitons (STEs) [41] which offer a route for swifter relaxation to the valence band. Whilst outside the scope of this letter, the difference between the response times can be understood in terms of the detailed

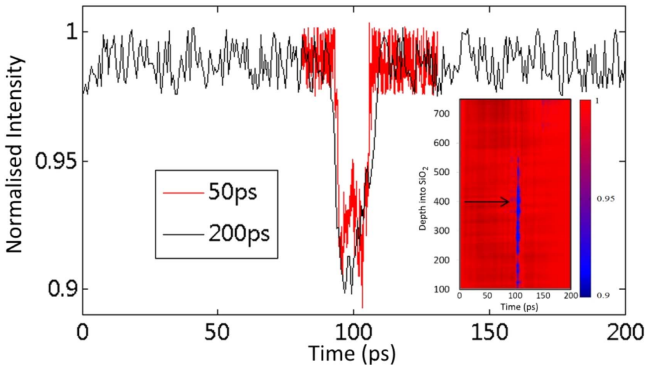

Figure 5. Optical streaking of ion induced opacity in SiO_2. The response of SiO_2 to the proton beam is detailed for probe beam durations of 50 ps (red) and 200 ps. Lineouts taken for energies of 8 MeV. SiO_2 displays a very rapid onset of opacity and recovery in comparison with the soda-lime glass sample. The entire interaction lasts around 20 ps which is more than an order of magnitude less than the soda-lime response. An increase in resolution for the 50 ps is clear and allows for better accuracy for samples with a shorter response. The inset is the raw image from the experiment for the 200 ps probe pulse.

composition of the two. SiO_2 is a highly pure form of glass whereas soda-lime silica is a multi-component glass where interstitial states between the conduction and valence bands of soda-lime slow the recombination of the electrons. STEs provide a pathway for swift recombination in SiO_2, hence the difference in recovery times.

For the rapid response that SiO_2 exhibits, utilising a shorter probe beam would increase the resolution of the measurement. A shorter duration probe ensures a higher resolution as a given pulse duration will span a greater range of frequencies in the images retrieved by the spectrometer. A full description of the resolution of this system is presented in the Methods section and figure 3. The red line in figure 5 illustrates the response of SiO_2 over a 50 ps window. Optical streaking over this window increases the resolution by a factor of four. Analysis of the highest energy protons ($\sim$10 MeV reveals a recovery time of 3.5 ± 0.7 ps meaning that even with a 200 ps probe pulse, we are still able to resolve the recovery of the sample from energy deposition of the highest energy protons. Measurements with the 50 ps pulse reveals the same main aspects of the material behaviour whilst giving a more sensitive temporal depiction of the interaction. Implementing a system whereby the probe beam can be altered to better resolve the dynamics from shot-to-shot is therefore of the utmost importance when investigating multiple samples with varying response times. The ability to do this with a fully synchronised proton pulse enables highly detailed temporal resolution for samples with even faster responses.

Discussion

Presented in this letter is a robust scheme of tracking ion damage in materials from high-energy, ultrashort ion pulses with picosecond laser pulses. Excitation of electrons across the 1 eV optical band gap of soda-lime silica and SiO_2 was observed and the subsequent recovery times were measured. The optical streaking process outlined has been shown as a means of resolving the dynamics in the sample over a range of sub-nanosecond temporal windows. This method is not limited to the dynamics induced by laser driven protons. Investigations of the effects on materials from other ions generated by high intensity laser interactions is also possible using this scheme. Utilisation of ultra-broadband probe pulses would allow for even greater temporal resolution of the ion induced dynamics. Although the materials detailed here are solely glass compounds, the extension of this method to observe the ultrafast response and consequent ion induced damage in a wide range of materials. Unlocking the effects of ion induced damage is key to implementing LDIA as a source of cancer therapy. Tracking the ultrafast dynamics in water is particularly crucial due to the high content of water in the human molecular composition as preventing damage to healthy cells surrounding cancerous tumours is a top priority for cancer treatments involving high energy radiation. Time-resolved studies of ultrafast proton induced processes such as the one presented here are an important step in understanding the dynamics of the earliest stages of this interaction. The flexibility of this scheme in terms of ease of setup and range of temporal resolution highlight its relevancy to this goal and by further application and testing the fundamental processes relevant to proton therapy can be directly studied.

Acknowledgments

The authors would like to acknowledge support for this work from the EPSRC through the following grants EP/L02327X/1, EP/K022415/1, EP/1031464/1 and EP/P016960/1.

Author contributions statement

BD and MZ conceived the experiment which was performed by MT, MC, GN, LS, DJ and BD. Data analysis and preparation of the manuscript was carried out by MC, BD, CLSL, MT and MZ. All authors reviewed the manuscript.

Additional information

The authors declare no competing financial interests.

ORCID iDs

M Coughlan https://orcid.org/0000-0002-6950-1896
D Riley https://orcid.org/0000-0002-6212-3212

References

[1] Dudovich N, Oron D and Silberberg Y 2002 Single-pulse coherently controlled nonlinear Raman spectroscopy and microscopy *Nature* **418** 512–4

[2] Maine P, Strickland D, Bado P, Pessot M and Mourou G 1988 Generation of ultrahigh peak power pulses by chirped pulse amplification *IEEE J. Quantum Electron.* **24** 398–403

[3] Backus S, Durfee C G, Murnane M M and Kapteyn H C 1998 High power ultrafast lasers *Rev. Sci. Instrum.* **69** 1207–23

[4] Mourou G A, Tajima T and Bulanov S V 2006 Optics in the relativistic regime *Rev. Mod. Phys.* **78** 309–71

[5] Dromey B *et al* 2006 High harmonic generation in the relativistic limit *Nat. Phys.* **2** 456

[6] Rödel C *et al* 2012 Harmonic generation from relativistic plasma surfaces in ultrasteep plasma density gradients *Phys. Rev. Lett.* **109** 125002

[7] Kiefer D *et al* 2013 Relativistic electron mirrors from nanoscale foils for coherent frequency upshift to the extreme ultraviolet *Nat. Commun.* **4** 1763

[8] Sarri G *et al* 2013 Laser-driven generation of collimated ultra-relativistic positron beams *Plasma Phys. Control. Fusion* **55** 124017

[9] Brabec T and Krausz F 2000 Intense few-cycle laser fields: Frontiers of nonlinear optics *Rev. Mod. Phys.* **72** 545–91

[10] Borghesi M 2014 Laser-driven ion acceleration: state of the art and emerging mechanisms *Nucl. Instrum. Methods Phys. Res.* A **740** 6–9

[11] Clark E L, Krushelnick K, Zepf M, Beg F N, Tatarakis M, Machacek A, Santala M I K, Watts I, Norreys P A and Dangor A E 2000 Energetic heavy-ion and proton generation from ultraintense laser-plasma interactions with solids *Phys. Rev. Lett.* **85** 1654–7

[12] Robinson A P L, Zepf M, Kar S, Evans R G and Bellei C 2008 Radiation pressure acceleration of thin foils with circularly polarized laser pulses *New J. Phys.* **10** 013021

[13] Krushelnick K *et al* 1999 Multi-MeV ion production from high-intensity laser interactions with underdense plasmas *Phys. Rev. Lett.* **83** 737

[14] Zepf M *et al* 2003 Proton acceleration from high-intensity laser interactions with thin foil targets *Phys. Rev. Lett.* **90** 064801

[15] Willingale L *et al* 2006 Collimated multi-MeV ion beams from high-intensity laser interactions with underdense plasma *Phys. Rev. Lett.* **96** 245002

[16] Esirkepov T, Borghesi M, Bulanov S V, Mourou G and Tajima T 2004 Highly efficient relativistic-ion generation in the laser-piston regime *Phys. Rev. Lett.* **92** 175003

[17] Henig A *et al* 2009 Radiation-pressure acceleration of ion beams driven by circularly polarized laser pulses *Phys. Rev. Lett.* **103** 245003

[18] Dromey B *et al* 2016 Picosecond metrology of laser-driven proton bursts *Nat. Commun.* **7** 10642

[19] Senje L *et al* 2017 Experimental investigation of picosecond dynamics following interactions between laser accelerated protons and water *Appl. Phys. Lett.* **110** 104102

[20] Cowan T E *et al* 2004 Ultralow emittance, multi-MeV proton beams from a laser virtual-cathode plasma accelerator *Phys. Rev. Lett.* **92** 204801

[21] Borghesi M, Fuchs J, Bulanov S V, Mackinnon A J, Patel P K and Roth M 2006 Fast ion generation by high-intensity laser irradiation of solid targets and applications *Fusion Sci. Technol.* **49** 412–39

[22] Schnurer M *et al* 2013 The beat in laser-accelerated ion beams *Phys. Plasmas* **20** 103102

[23] Bulanov S V and Khoroshkov V S 2002 Feasibility of using laser ion accelerators in proton therapy *Plasma Phys. Rep.* **28** 453–6

[24] Roth M *et al* 2001 Fast ignition by intense laser-accelerated proton beams *Phys. Rev. Lett.* **86** 436

[25] Audebert P *et al* 1994 Space-time observation of an electron gas in SiO_2 *Phys. Rev. Lett.* **73** 1990–3

[26] Horn A, Kreutz E W and Poprawe R 2004 Ultrafast time-resolved photography of femtosecond laser induced modifications in BK7 glass and fused silica *Appl. Phys.* A **79** 923–5

[27] Pelka A *et al* 2010 Ultrafast melting of carbon induced by intense proton beams *Phys. Rev. Lett.* **105** 265701

[28] Correa A A, Kohanoff J, Artacho E, Sánchez-Portal D and Caro A 2012 Nonadiabatic forces in ion-solid interactions: the initial stages of radiation damage *Phys. Rev. Lett.* **108** 213201

[29] Rigaud O, Fortunel N O, Vaigot P, Cadio E, Martin M T, Lundh O, Faure J, Rechatin C, Malka V and Gauduel Y A 2010 Exploring ultrashort high-energy electron-induced damage in human carcinoma cells *Cell Death Dis.* **1** e73

[30] Chitose N, Katsumura Y, Zuo Z, Domae M, Ishiqure K and Murakami T 1997 Radiolysis of aqueous solutions with pulsed helium ion beams: yield of $(SCN)_2^-$ formed by scavenging OH as a function of SCN^- concentration *J. Chem. Soc., Faraday Trans.* **93** 3939–44

[31] Dzelzainis T *et al* 2010 The TARANIS laser: a multi-terawatt system for laser-plasma investigations *Laser Part. Beams* **28** 451–61

[32] Yin L, Albright B J, Hegelich B M and Fernandez J C 2006 GeV laser ion acceleration from ultrathin targets: the laser break-out afterburner *Laser Part. Beams* **24** 291–8

[33] Qiao B, Zepf M, Borghesi M and Geissler M 2009 Stable GeV ion-beam acceleration from thin foils by circularly polarized laser pulses *Phys. Rev. Lett.* **102** 145002

[34] Passoni M, Bertagna L and Zani A 2010 Target normal sheath acceleration: theory, comparison with experiments and future perspectives *New J. Phys.* **12** 045012+

[35] LaVerne J A 2000 Track effects of heavy ions in liquid water *Radiat. Res.* **153** 487–96

[36] Tavernier S 2009 Interactions of particles in matter *Experimental Techniques in Nuclear and Particle Physics* (Berlin: Springer) pp 23–53

[37] Marjoribanks R S, Jaanimagi P A and Richardson M C 1986 Principles of streak and framing photography by frequency-encoding on a chirped pulse *Proc. SPIE* **0693** 13

[38] Polli D, Brida D, Mukamel S, Lanzani G and Cerullo G 2010 Effective temporal resolution in pump-probe spectroscopy with strongly chirped pulses *Phys. Rev.* A **82** 053809

[39] Wigner E 1932 On the quantum correction for thermodynamic equilibrium *Phys. Rev.* **40** 749–59

[40] Hong K H, Kim J H, Kang Y H and Nam C H 2002 Time-frequency analysis of chirped femtosecond pulses using Wigner distribution function *Appl. Phys.* B **74** s231–6

[41] Isail-Beigi S and Louie S G 2005 Self-trapped excitons in silicon dioxide: mechanism and properties *Phys. Rev. Lett.* **95** 156401

[42] Ziegler J F, Ziegler M D and Biersack J P 2010 SRIM—the stopping and range of ions in matter (2010) *Nucl. Instrum. Methods Phys. Res.* B **268** 1818–23